Library, L.M.A.L.

541
171

TECHNICAL MEMORANDUMS

NATIONAL ADVISORY COMMITTEE FOR AERONAUTICS

No. 789

TURBULENT JET EXPANSION

By E. Förthmann

Ingenieur-Archiv, Vol. V, No. 1, 1934

Washington
March 1936

NATIONAL ADVISORY COMMITTEE FOR AERONAUTICS

TECHNICAL MEMORANDUM NO. 789

TURBULENT JET EXPANSION*

By E. Förthmann

SUMMARY

The investigation described in this report was made to study the velocity distribution in an open, in a partially open, and in a partially expanding jet. The open-jet observations reveal minor systematic discrepancies from Tollmien's theoretical velocity distribution. The shearing-stress distribution for the partially open jet was determined. The value derived for the ratio of mixing distance to jet width was found to be in close agreement with the corresponding value for the open-jet boundary. The streamline pattern in a partially expanding channel was obtained from the observed velocity distribution and plotted, after which the distribution of the mixing distance for this case was also ascertained.

INTRODUCTION

Based on Professor Prandtl's equation for the apparent shearing stress induced by turbulent momentum interchange (reference 1)

$$\tau_{xy} = \rho\, l^2 \left|\frac{\partial u}{\partial y}\right| \frac{\partial u}{\partial y} \qquad (1)$$

(where u = mean velocity in x direction; y = velocity at right angles to it; ρ = density; and l = mixing distance), W. Tollmien (reference 2) has analyzed various cases of free turbulence - i.e., of flows without boundary walls. Now the purpose of the present investigation was to experimentally check one of his examples: the uniplanar jet expansion upon emergence from a linear slot, and to prove the proportionality constant c, which he introduced as

$$l = c\,x \qquad (2)$$

*"Über turbulente Strahlausbreitung." Ingenieur-Archiv, vol. V, no. 1, 1934, pp. 42-54.

in his article. (The corresponding laminar problem has been theoretically analyzed by H. Schlichting, in Zeitschrift für angewandte Mathematik und Mechanik, No. 13, 1933, p. 260; see also W. Müller, in the same issue, p. 395.) In addition, the case of turbulent expansion in a partially open and in a partially expanding jet, were to be checked by the same methods.

EXPERIMENTAL ARRANGEMENT

Tollmien's example treats the uniplanar jet expansion, to wit: an air stream emerging through an assumedly linear slot intermingling with still air. The assumption of linear slot is, of course, not exactly realizable in an experiment, although a slot having a height equal to twenty times its breadth, approaches this condition fairly closely (fig. 1). A simple calculation then affords a linear slot in extrapolation. To render the problem amenable to uniplanar treatment, it was necessary to provide such flow conditions, for which the velocity distribution was the same in all horizontal sections (as far as the upper and lower limit range). Compliance with this premise was demanded from the second and third cases also. For the first case - that is, perfectly free jet expansion - the two-dimensionality was summarily predetermined, whereas in the other two cases, it was more difficult. However, before going into details, it is advisable to describe the experimental set-up itself.

The air is supplied by a two-stage blower. A honeycomb is mounted at G, while aft of it the circular section merges into a rectangular pressure chamber which gradually tapers to a slot S. This part of the equipment served in all experiments, although in the second and third cases some other parts were added. A lateral orifice on the pressure chamber D connects with a manometer, which is held constant by continuous regulation of the r.p.m. of the motor, thus insuring a constant air volume in the pressure chamber as well as through the slot. The actual test section - after passage of slot - was, in the first case, the free air space before the slot. Thus, the first problem consisted in dividing this space into exact coordinates, so as to be able to measure it point by point. This was accomplished with the support shown in figure 2. A small table mounted on two parallel posts can be raised

or lowered. A horizontal balance bar attached to the little table, supports, on its end, the pressure survey apparatus intended to indicate the pressure at the particular point of the air space. The survey apparatus connects, by means of a pipe running through the balance bar, with a rubber tubing which, fastened at the other end of the bar, leads to the manometer. The two uprights are mounted on a heavy metal support which rests on four setscrews on a wooden base. The latter rests only with the four corners on the floor, whereby one corner itself is replaced by a setscrew to allow for the unevenness of the floor. The setscrews of the metal base assure perfect perpendicularity of the uprights. The bar carrying the pressure survey device, a pitot tube, was at first set into severe oscillations by the air stream, but these could be almost completely removed, after various attempts, by the damping D. This is effected through a loose piece of metal placed on the bar linked to an inclined rocker at a fixed point and which slides back and forth with friction when the bar oscillates. The origin of the coordinate system of the test range was placed in the intersection of the diagonals of the slot for reasons of symmetry of the whole test field - direction x in flow direction, direction y, horizontal and perpendicular to it. In direction z (vertical), the pressure grading was, as stated before, constant.

The total head was recorded by pitot tube and Prandtl type manometer. The static pressure was recorded with a tube having lateral orifices and an inclined manometer. From the resultant dynamic pressure, the velocity distribution was computed after correcting for air pressure and temperature. In the second test the creation of a two-dimensional flow was, of course, extremely difficult. The original shape of the channel was as shown in figure 3. But, this arrangement proved unsuitable, because the suction of the still air, conditioned by the air stream, forced it to be sucked around the upper and lower edges and the thus-created vortices at the edges soon destroyed the uniformity of flow in the vertical.

This objectionable feature was removed by fitting the curved pieces of metal shown in figure 4. Even so, there remained difficulties despite the careful alinement of the boundary walls (by means of a light beam), until the slot was narrowed from 6.5 to 3 cm (2.56 to 1.18 in.) for a height of 65 cm (25.6 in.), and a second close-meshed screen was inserted between pressure chamber and slot. This finally insured a satisfactory velocity distribution in the vertical (fig. 5).

For the first and second experiments, it was very desirable to be able to adjust both pitot and static tube in the pertinent flow direction at the extreme mixing boundary between jet and inducted air, where the flow direction deflects considerably from that of the principal flow (x direction). The tube had to be made to pivot about the test point. The necessary device as shown in figure 6, includes a balance bar with a scale division at its outer end. Then the static tube, which is very responsive to directional changes, was rotated until it indicated maximum pressure, after which the corresponding angular setting was recorded and the pitot tube pointed in the same direction for the total-head measurement. After thus solving most of the experimental problems, there still remained the difficult feat of attaining a satisfactory static pressure reading.

Static Pressure

The static pressure was recorded, as previously stated, with a pitot tube having four symmetrical orifices on the sides (fig. 7). It was soon found that this tube recorded a very marked negative pressure, amounting up to 15 percent of the dynamic pressure in the main mixing zone of air stream and still air, as against one-half percent and, at that, indicative of positive pressure, according to Tollmien's theory. Consequently, these measurements, rather than representing real values, imply that survey devices of this type do not record the real static pressure in turbulent flow. They are extremely responsive to directional changes, and even a change of a few degrees causes a pressure drop in the manometer, which is no longer in accord with actual pressure conditions in the jet.

Since, in turbulent flow, there is a continuous change in flow direction, of the individual fluid particles toward the main flow direction, the manometer reading is lower than the true static pressure. And this figure is so much less as the turbulent interchange is greater - hence the premise, confirmed by personal observational study, appears justified. That is, a survey apparatus of this kind indicates a minimum of the pressure at the points of maximum interchange and consequently, gives the point of maximum shearing stress, but for the rest, is totally unsuitable for recording the actual static pressure in turbulent flow (reference 3).

The next step was to design a device which was not re-

sponsive to changes of flow direction. After various abortive attempts, the form shown in figure 8 was adopted. The static pressure tap was placed within a turned-up hollow cylinder, whose walls were hollow and served as pressure leads to the manometer. A calibration for directional change revealed it to be unaffected by flow direction over a range of approximately 80°; that is, the reading was the same after being turned through a $\pm 40^{\circ}$ angle relative to the main flow direction (fig. 9).

On the other hand, it was still markedly influenced by the dynamic pressure (fig. 10) which, of course, decreases as the air speed increases. Since most measurements were made at such speeds, when the effect of dynamic pressure is small, the order of magnitude of the static pressure was obtainable to such a degree as to make the static pressure effect amenable to estimation when computing the shearing stresses.

The interaction of the static pressure on the shearing stress calculation could be disregarded in first approach (as proved elsewhere), hence it afforded a more exact determination of the static pressure in our particular case. In any case, it appears to be desirable, however, to concentrate on the design of a survey apparatus which, totally unaffected by main flow direction and amount of dynamic pressure, affords an unobjectionable static pressure reading.

RESULTS OF TESTS

Open Jet

The thus-obtained velocity distributions for various slot spacings a are shown in figure 11. These profiles are plotted nondimensionally in figure 12 after dividing the pertinent velocities by the velocity maximum of the particular profile and the related position coordinate by the coordinate of the halved maximum velocity.

The velocity profiles may be expressed by

$$u = x^{p} f_1 \left(\frac{y}{x^{q}}\right)$$

Comparing two profiles each for the constants p and

q, we have:

$$p = -0.50, \qquad q = 0.997$$

in accord with the theory which stipulates $p = -\frac{1}{2}$, $q = +1$.

For comparison with Tollmien's theoretical velocity distribution, we included his theoretical curve in figure 12.. Both the theoretical and experimental curves have been normalized so as to be agreeable in the points $y = 0$, $u = u_{max}$ and $y = y\left(\frac{u_{max}}{2}\right)$, $u = \frac{u_{max}}{2}$.

Approaching maximum velocity, the measured velocity is seen to be higher, and at the jet boundary lower, than the theoretical. The same phenomenon was observed in the rotationally symmetrical wake (unpublished measurements by Nikuradse and Schlichting). The proportionality constant c in the mixing distance equation $l = c\,x$ was defined* at $c = 0.0165$, which gives $\frac{l}{b} = 0.066$, when $2b$ = total jet width.

Partially Open Jet

The obtained velocity profiles for different slot distances a are shown in figure 13. Whereas the first three profiles (a = 10, 20, and 35 cm (3.94, 7.87, and 13.78 in.)) still show a slot-width effect and therefore do not count in the final evaluation, the others, farther away, do not reveal it. At the same time it was important to know whether these profiles were mutually similar and the flow thus followed a simple law within the entire range. The procedure was the same as for the open jet. The individually recorded velocity was divided by its momentary maximum of the profile, and the individual position coordinates by the coordinate of the velocity which, on the free side of the profile, equals half the velocity maximum. The thus-obtained nondimensional values for the individual profiles were plotted on one sheet. It was found that all profiles are coincident in one curve (fig. 14), thus proving that the flow in this case also follows a simple law of similitude within the entire range.

---

*Owing to the reduction of the finite slot width to linear slot, we have $x = a + e$ (a = distance from slot, $e = -4.5$ cm (17.7 in.).

The comparison of two adjacent profiles gave:

$$u = x^{-\frac{1}{2}} f_2 \left(\frac{y}{x^{0.99}}\right)$$

consequently, $p = -\frac{1}{2}$, $q = 0.99$

Hereby it was necessary to so reduce the distance from the slot of finite width to a linear slot, that a constant value e was added to distance a, making the theoretical distance $x = a + e$. The values for p, q, and e were defined as follows: Since the individual profiles are coincident, the momentary velocity must be dependent on the theoretical slot distance as well as on a function which refers the jet width to this distance. That is,

$$u = x^p f_2 \left(\frac{y}{x^q}\right)$$

holds again, with

$$x = a + e$$

a being the measured distance from the slot, e the above-cited constant additive length. Now, since the maximum velocity is simply a function of the slot distance, the equation

$$\frac{(a_1 + e)^p}{(a_2 + e)^p} = \frac{u_m (a_1)}{u_m (a_2)}$$

must hold; whereby a_1 and a_2 are the measured distances of profiles 1 and 2 from the slot, and $u_m (a_1)$ and $u_m (a_2)$, the maximum velocities of profiles 1 and 2. Likewise, it must be

$$\frac{(a_2 + e)^p}{(a_3 + e)^p} = \frac{u_m (a_2)}{u_m (a_3)}$$

for profiles 2 and 3.

From these equations, e and p are then computed at

$$e = 20.1 \text{ cm } (7.9 \text{ in.}), \quad p = -\frac{1}{2}$$

q may also be expressed by an equation, for according to the law of similitude for velocity distribution, equal $\frac{y}{(a+e)^q}$ values have equal $\frac{u}{u_m}$ values. The selection of points in two profiles, so that $\frac{u}{u_m} = \frac{1}{2}$, stipulates

$$\frac{y\,(a_1)}{y\,(a_2)} = \frac{(a_1+e)^q}{(a_2+e)^q}$$

when $y\,(a_1)$ and $y\,(a_2)$ denote the y coordinates of points $\frac{u}{u_m} = \frac{1}{2}$. From this q may be computed. Even so, the obtained value cannot be considered final because the shape of the velocity profile is dependent on the wall friction as well as on the mixing with the still air. Both processes must be treated separately. Substituting for this y, measured with inclusion of the friction zone, the distance of that point on the free side where the velocity equals $\frac{3}{4}\,u_{max}$ and $\frac{1}{4}\,u_{max}$, say, at points 1 and 2, removes the wall-friction effect. In this manner the value $q_1 = 0.997$ was obtained.

A logarithmic plot of the velocities versus y for wall proximity, reveals a rise of the velocity with the 1/7 power of the wall distance, while for this zone $q_2 = 0.8995$.

This value for q_2 can also be deduced theoretically. It has been shown that

$$u = c\,y^{1/7} \tag{3}$$

is valid. On the other hand, v. Karman (reference 4) defined the shearing stress at the wall with

$$\tau_0 \sim \rho\,\nu^{1/4}\,c^{7/4} \tag{4}$$

($\sim$ = proportional, ν = kinematic viscosity)

The momentum theory (equation (9)) stipulates

$$\tau_0 \sim \rho\,\frac{u^2\,y}{x} \tag{5}$$

Then it is

$$u = x^p f(\eta), \quad \text{where} \quad \eta = \frac{y}{x^q} \tag{6}$$

that is, with $y = x^q \eta$

$$\tau_o \sim \rho \frac{x^{2p} f^2(\eta) x^q \eta}{x}$$

or

$$\frac{\tau_o}{\rho} \sim x^{2p+q-1} \tag{7}$$

To render (3) agreeable with (6) it must be

$$u \sim x^p \left(\frac{y}{x^q}\right)^{1/7}$$

for wall proximity,

or

$$c \sim x^{p-\frac{q}{7}}$$

which, written in (4) gives:

$$\frac{\tau_o}{\rho} \sim \nu^{\frac{1}{4}} x^{\frac{7}{4}\left(p-\frac{q}{7}\right)} \tag{8}$$

From (7) and (8) then follows

$$x^{2p+q-1} \sim x^{\frac{7}{4}\left(p-\frac{q}{7}\right)}$$

or

$$\left(2 - \frac{7}{4}\right) p + q \left(1 + \frac{1}{4}\right) - 1 = 0$$

that is,

$$q = \frac{4}{5} - \frac{p}{5}$$

The insertion of the ascertained value $p = -\frac{1}{2}$, then actually affords

$$q = q_2 = 0.9$$

Calculation of Shearing Stress

According to the first equation of motion, it is

$$u \frac{\partial u}{\partial x} + v \frac{\partial u}{\partial y} = - \frac{1}{\rho} \frac{\partial p}{\partial x} + \frac{1}{\rho} \frac{\partial \tau}{\partial y}$$

Integration, according to y gives:

$$\frac{\tau}{\rho}\Big|_0^y = \int_0^y \left(u \frac{\partial u}{\partial x} + v \frac{\partial u}{\partial y} \right) dy + \frac{1}{\rho} \int_0^y \frac{\partial p}{\partial x} dy$$

$$= \int_0^y u \frac{\partial u}{\partial x} dy + vu\Big|_0^y - \int_0^y \frac{\partial v}{\partial y} u dy + \frac{1}{\rho} \int_0^y \frac{\partial p}{\partial x} dy$$

which, because $\frac{\partial v}{\partial y} = - \frac{\partial u}{\partial x}$, becomes

$$\frac{\tau}{\rho}\Big|_0^y = 2 \int_0^y u \frac{\partial u}{\partial x} dy + vu\Big|_0^y + \frac{1}{\rho} \int_0^y \frac{\partial p}{\partial x} dy$$

which may also be written:

$$\frac{\tau}{\rho}\Big|_0^y = \frac{\partial}{\partial x} \int_0^y u^2 dy - u \frac{\partial}{\partial x} \int_0^y u dy + \frac{1}{\rho} \int_0^y \frac{\partial p}{\partial x} dy \qquad (9)$$

The differentiation according to x may, on the basis of the law of similitude for velocity distribution

$$u = x^p f(\eta)$$

be effected with $\eta = \frac{y}{x^q}$.

Disregarding the pressure term which, according to the measurements, is so small as to be negligible for the shearing stress calculation, affords

$$\frac{\tau}{\rho}\Big|_0^y = \frac{\partial}{\partial x} [x^{2p} \int_0^y f^2 dy] - x^p f \frac{\partial}{\partial x} x^p \int_0^y f dy$$

$$= (2p+q)\, x^{2p+q-1} \int_0^\eta f^2 d\eta - q \eta\, x^{2p+q-1} f^2\Big|_0^\eta$$

$$- x^p (p+q)\, x^{p+q-1} f \int_0^\eta f d\eta + q \eta\, x^{2p+q-1} f^2\Big|_0^\eta$$

$$= (2p+q)\, x^{2p-1} \int_0^y f^2 dy - (p+q)\, x^{2p-1} f \int_0^y f dy$$

Thus the shearing stress formula for any value of p and q becomes:

$$\frac{\tau}{\rho}\Big|_0^y = \frac{1}{x}\left[(2p + q)\int_0^y u^2 dy - (p + q)\, u \int_0^y u dy\right] \qquad (10)$$

With y_m as coordinate of the velocity maximum u_m, gives for the wall region $0 \leq y \leq y_m$ with $p = -\frac{1}{2}$ and $q = 0.9$

$$\frac{\tau}{\rho}\Big|_0^y = -\frac{0.1}{x}\left[\int_0^y u^2 dy + 4u \int_0^y u dy\right] \qquad (11)$$

and for the outside zone $y \geq y_m$ with $p = -\frac{1}{2}$, $q = 1.0$:

$$\frac{\tau}{\rho}\Big|_{y_m}^y = -\frac{1}{2x}\, u \int_{y_m}^y u dy \qquad (11a)$$

From (11) and (11a) follows the shearing stress in the outside zone at

$$\frac{\tau}{\rho}\Big|_0^y = -\frac{0.1}{x}\left[\int_0^{y_m} u^2 dy + 4u_m \int_0^{y_m} u dy + 5u \int_{y_m}^y u dy\right] \qquad (12)$$

Equations (11) and (12), containing only known values, served as basis of the shearing stress calculation.

The values of the integrals at the particular points y were graphically integrated. The resulting τ/ρ values give the difference in shearing stress at any point of the flow from the corresponding wall figure which is not zero; although the shearing stress at the jet edge relative to the free space must become zero. Plotting the values accordingly reveals the shearing stress as passing through zero at the point of maximum flow velocity, as equally follows from equation (12). This is readily understood because at this point the shear due to wall friction, as well as that due to mixing, must disappear. In figure 15 the shear distribution is shown plotted against jet width.

Calculation of Mixing Distance

Following the determination of the shearing stress, the mixing distance was computed according to

$$\frac{\tau}{\rho} = l^2 \left|\frac{\partial u}{\partial y}\right| \frac{\partial u}{\partial y}$$

The $\frac{\partial u}{\partial y}$ values were obtained by graphical differentiation of the curves established for the velocity distribution in y direction. The value for the partially open jet is

$$\frac{l}{b} = 0.0684$$

Here b = width of mixing zone - that is, exclusive of friction zone on the fixed wall. This figure is fairly agreeable with that for the free jet boundary $\left(\frac{l}{b} = 0.0682\right)$, given in Tollmien's cited report.

Flow in Partially Expanding Jet

Experimentally, this case is not unlike that of the others except for the closing of the fourth side of the previous three-sided channel. The balance bar carrying the pressure survey apparatus was inserted through openings into the newly installed side wall of the channel. The openings for different slot spacings harmonized exactly with the profile of the balance bar. The unused openings were carefully plugged. The measurements included the total head and the static pressure in eight sections, affording the velocity distribution in the channel for the different slot spacings* (fig. 16). Individual graphical integration of the velocity profiles then gave the volume of flow for each. The points of equal flow volume were then connected, resulting in the flow pattern shown in figure 17.

Lastly, we computed the mixing distance for the case of abruptly expanding channel. The velocity profiles being no longer similar, the calculation of the mixing distance had to be made on the basis of the general equation (9). The shearing stress τ_o at the wall was computed

---

*The measured velocity profiles reveal "bulges" near the points where the prefix of the velocity changes. This is due to the fact that at the point where the turbulent velocity fluctuation is of the same order of magnitude as the mean velocity, the determination of the velocity from pitot-tube readings is considerably falsified; that is, the velocity is always too high. For the subsequent evaluations, this error was minimized by plotting the velocity profiles smooth in the vicinity of the zero points. (Compare the dashed lines in fig. 16.)

from the 1/7 power law for velocity distribution at

$$\tau_o = 0.0225 \frac{\rho u^2}{2} \left(\frac{\nu}{uy}\right)^{1/4}$$

The integral in (9) was defined graphically from the measured velocity distributions. Thus figure 18 illustrates the obtained distribution of the mixing distance over the section for five velocity profiles at distances a = 10 to a = 60 cm (a = 3.94 to 23.62 in.) from the discharge opening. The notable fact here is that in the vicinity of the wall the mixing distance increases considerably more with the wall distance than in the usual channel or pipe flow, where $l = 0.4\ y$ (reference 6) in wall proximity. It does therefore seem of importance as far as the mechanism of turbulence is concerned, whether the air sucked in and carried along by the jet was at rest as in both the open and in the partially open jet, or whether the air was already in turbulent motion beforehand, as was the case here. At greater wall distance the mixing distance assumes a constant and practically equal value for all profiles; that is, $l \approx 1.3$ cm (0.51 in.) and, since b = 18 cm (7.09 in.),

$$\frac{l}{b} = 0.072$$

b = total channel breadth. (The value for the straight pipe is $\left(\frac{l}{d}\right)_{max} = 0.07$ for pipe center - that is, almost the same.

This method of computing the mixing distance is no longer permissible for profiles at greater distances from the exit opening because the simple mixing distance formula (1) no longer holds, as a result of the considerable directional differences of the individual streamlines. As for the rest, the determination of the mixing distance by this method can lay no great claim to accuracy, because the flow was not strictly two-dimensional, and the flow volume therefore was different in the individual sections - a fact which is felt particularly disturbing in the graphical differentiation, according to x. Even so, it may be seen that the mixing distance in the suddenly expanding channel is of the same order of magnitude as for the open and the partially open jet.

In conclusion, the writer wishes to acknowledge his indebtedness to Professor Prandtl for suggesting the investigation, and for his valuable assistance; and to Dr. W. Tollmien and Dr. H. Schlichting, for their critical reading of the manuscript.

Translation by J. Vanier,
National Advisory Committee
for Aeronautics.

REFERENCES

1. Prandtl, L.: Bericht über Untersuchungen zur ausgebildeten Turbulenz. Z.f.a.M.M., vol. 5, no. 2, April 1925, p. 136; und Verh. 2. int. Kongr. techn. Mech., Zurich, 1926, p. 62.

2. Tollmien, W.: Berechnung turbulenter Ausbreitungsvorgänge. Z.f.a.M.M., vol. 6, no. 6, December 1926, p. 468.

3. Schlichting, H.: Ing.-Archiv, vol. 1, 1930, p. 537.

4. Karman, Th. v.: Über laminare und turbulente Reibung. Z.f.a.M.M., vol. 1, no. 4, August 1921, p. 233.

5. Gruschwitz, E.: Ing.-Archiv, vol. 2, 1931, p. 341.

6. Karman, Th. v.: Mechanical Similitude and Turbulence. T.M. No. 611, N.A.C.A., 1931.

Nikuradse, J.: Gesetzmässigkeiten der turbulenten Strömung in glatten Rohren. V.D.I.-Forsch.-Heft, 1932, p. 356

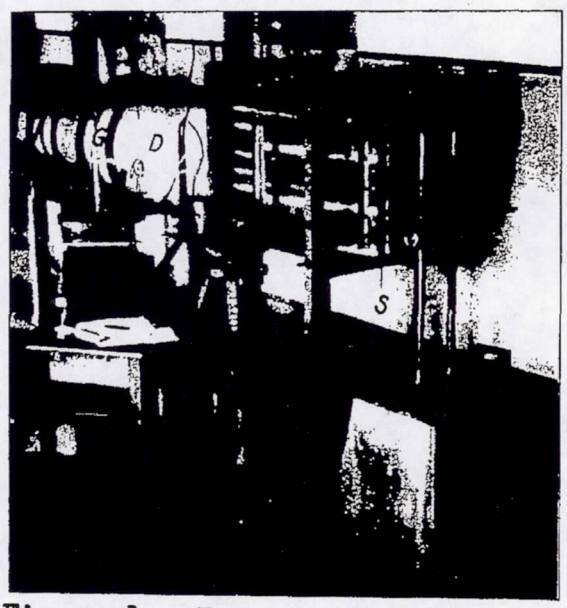

Figure 1.- Experimental layout for open jet measurements.(Blower with slot-shaped contraction.)

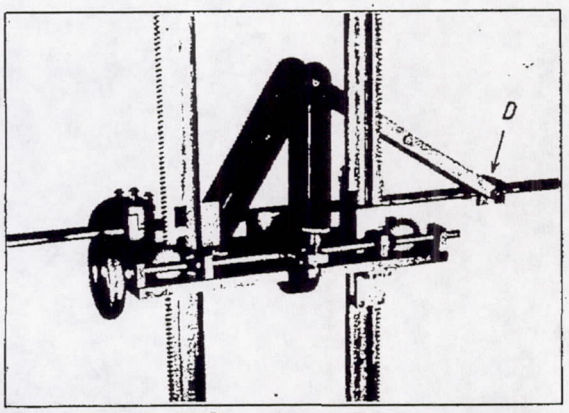

Figure 2.- Carrier for pressure survey apparatus.

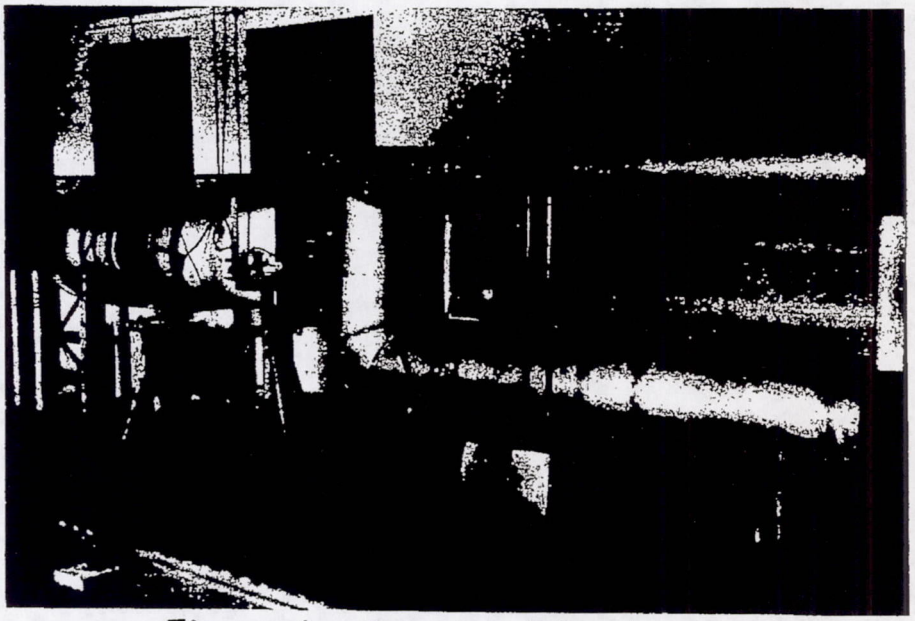

Figure 4.- Experimental setup for partially open jet.

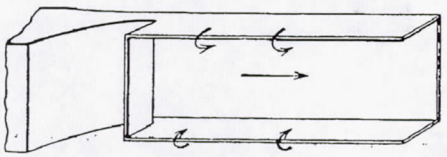

Figure 3.- Partially open jet.

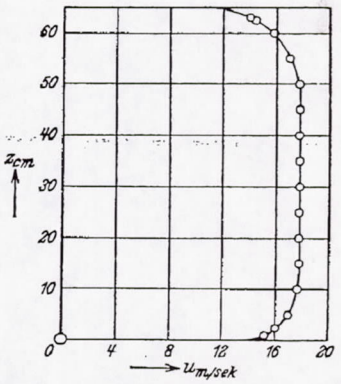

Figure 5.- Velocity distribution at right angles to main flow plane for partially open jet.

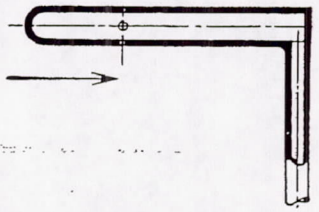

Figure 7.- Static tube with side orifices.

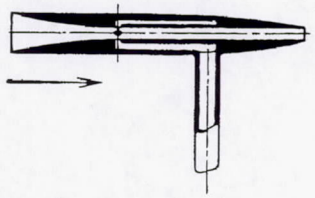

Figure 8.- Static pressure tube with inside holes.

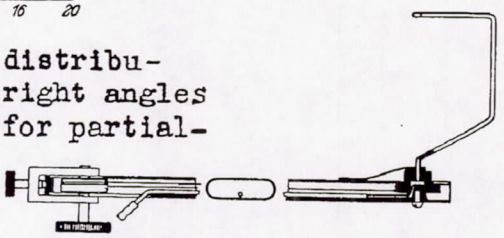

Figure 6.- Device for rotating the pressure survey apparatus about the vertical axis.

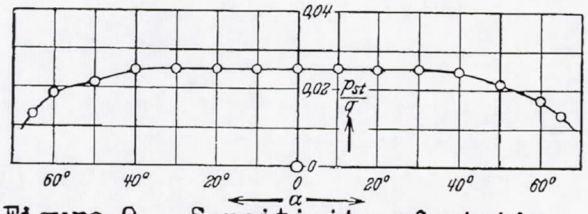

Figure 9.- Sensitivity of static tube.

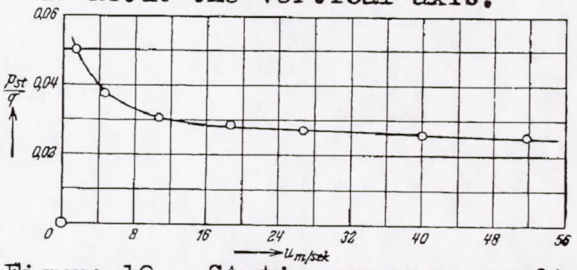

Figure 10.- Static pressure reading against air speed.

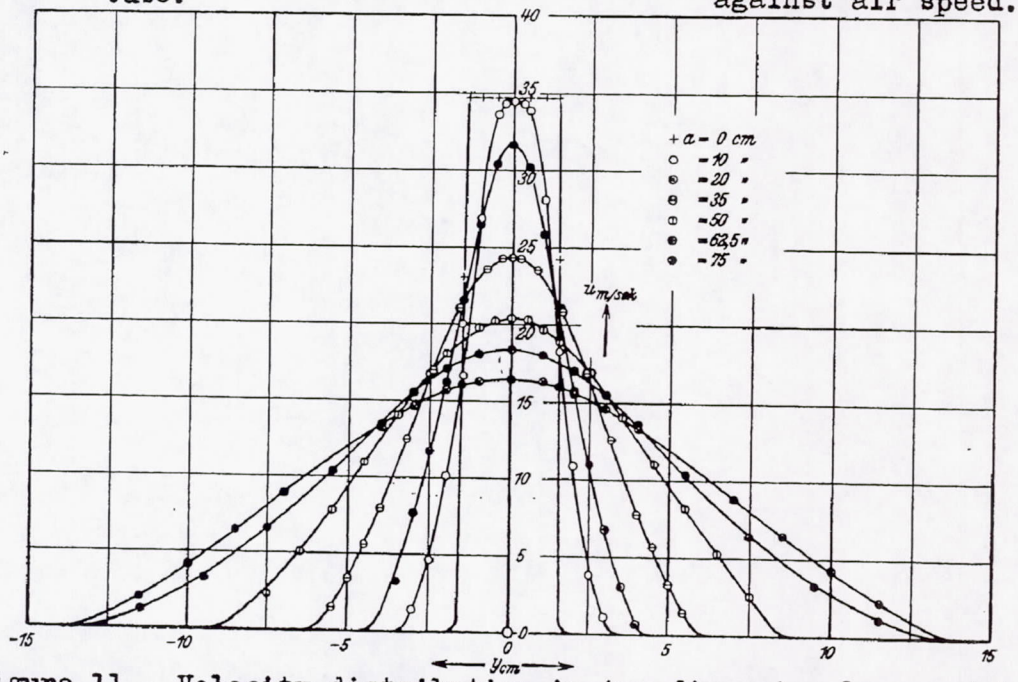

Figure 11.- Velocity distribution in two-dimensional open jet for different distances from the slot.

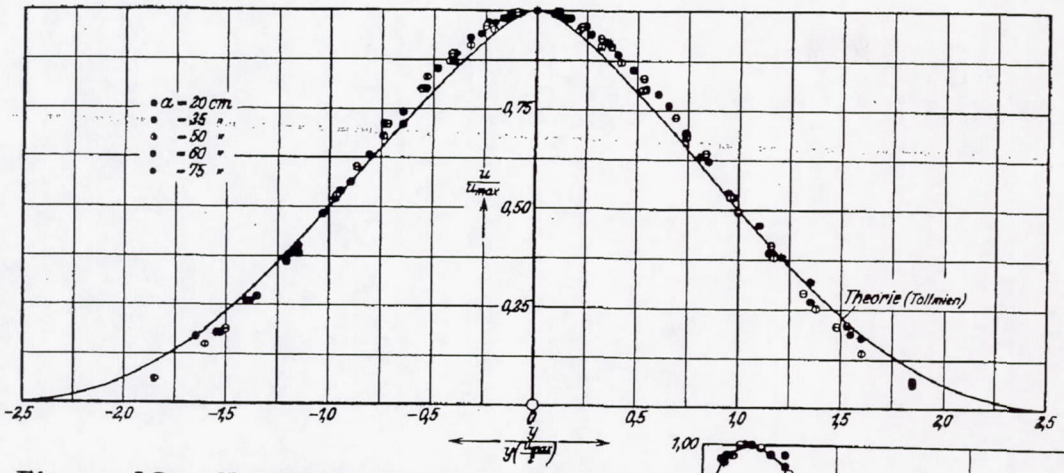

Figure 12.- Non-dimensional velocity distribution in two-dimensional open jet.

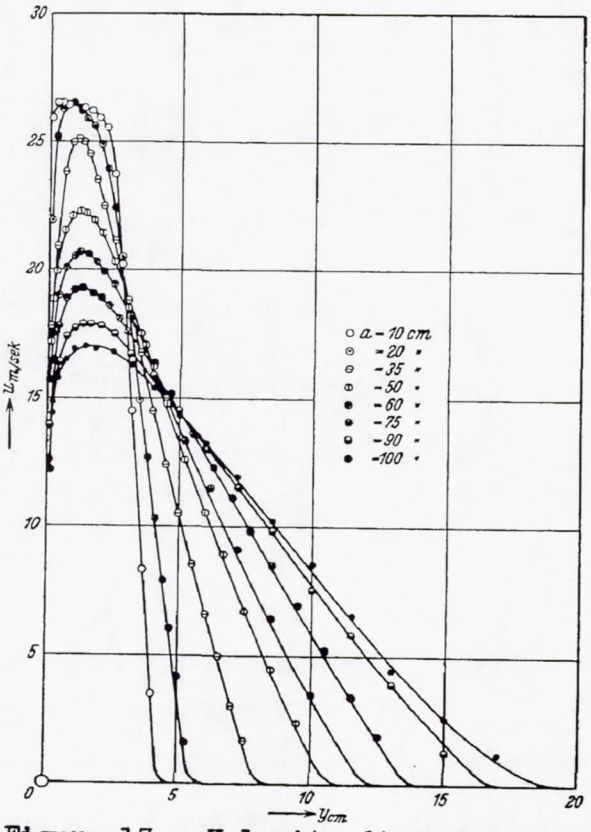

Figure 13.- Velocity distribution in partially open jet for different distances from the slot.

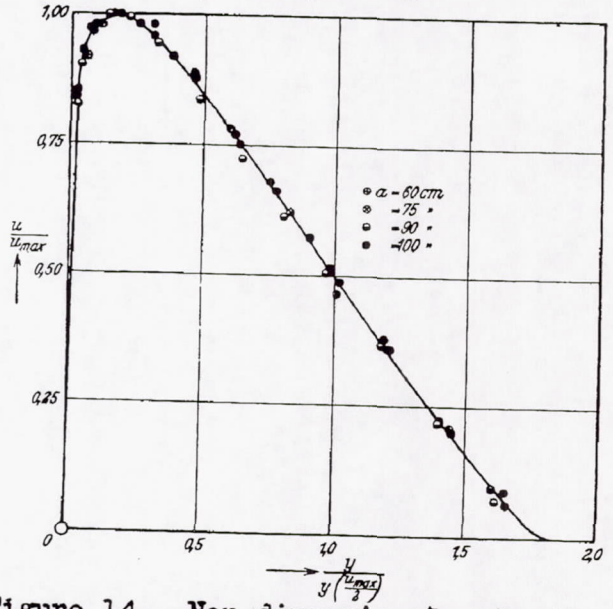

Figure 14.- Non-dimensional velocity distribution in partially open jet.

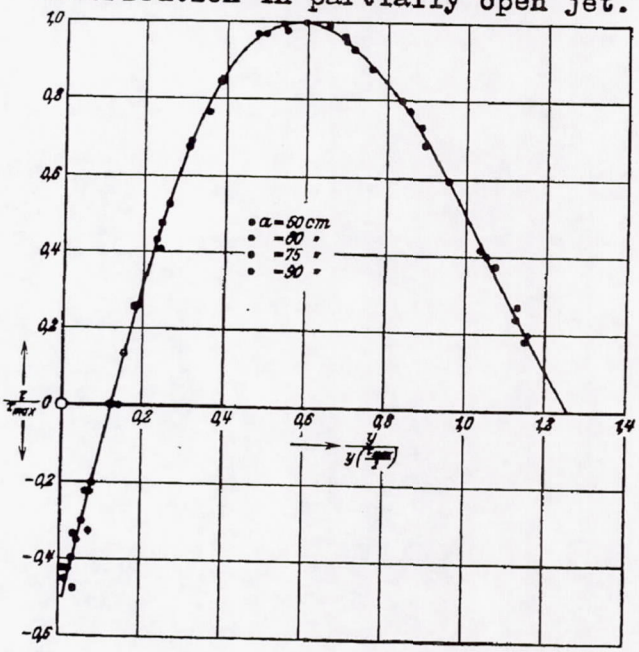

Figure 15.- Shear distribution in partially open jet.

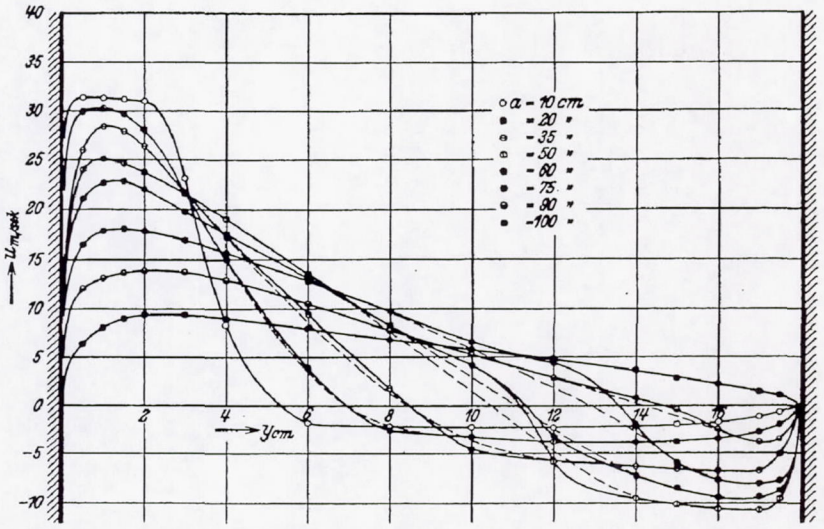

Figure 16.- Velocity distribution in partially expanding jet for different distances from the slot.

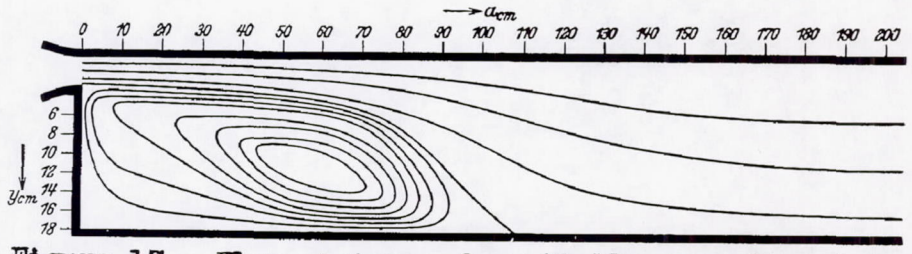

Figure 17.- Flow picture of partially expanding jet.

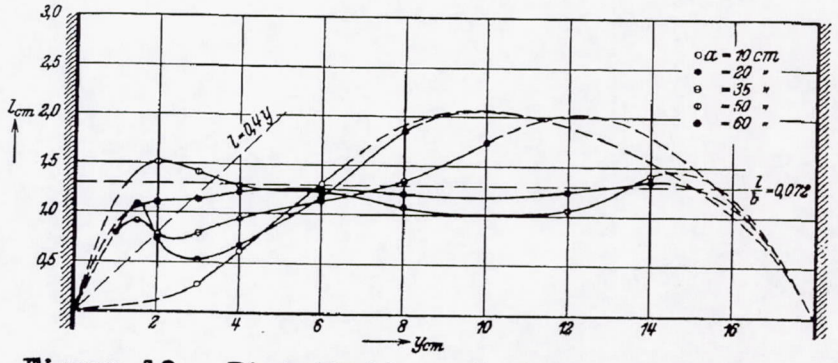

Figure 18.- Distribution of mixing distance in partially expanding channel.